Magnetoelectronic phase separation in $La_{1-x}Sr_xCoO_3$ single crystals: Evidence from critical behavior

N. Khan,[1] P. Mandal,[1] K. Mydeen,[2] and D. Prabhakaran[3]

[1]*Saha Institute of Nuclear Physics, 1/AF Bidhannagar, Calcutta 700 064, India*

[2]*Centre for High Pressure Research, School of Physics, Bharathidasan University, Tiruchirappalli 620 024, India*

[3]*Clarendon Laboratory, Department of Physics, University of Oxford, Oxford OX1 3PU, United Kingdom*

(Received 16 December 2011; revised manuscript received 27 March 2012; published 14 June 2012)

We have investigated the critical behavior of ferromagnetic $La_{0.75}Sr_{0.25}CoO_3$ and $La_{0.79}Sr_{0.21}CoO_3$ single crystals from the bulk magnetization measurements around their Curie temperature (T_C). The detailed analysis of the dc magnetization data using different techniques such as the Kouvel-Fisher, the Arrott-Noaks, and critical isotherm plots yield the critical exponents of $\beta = 0.362 \pm 0.002$, $\gamma = 1.304 \pm 0.006$, and $\delta = 4.75 \pm 0.01$ with $T_C = 213.93 \pm 0.02$ K for $La_{0.75}Sr_{0.25}CoO_3$ and $\beta = 0.491 \pm 0.004$, $\gamma = 1.217 \pm 0.003$, and $\delta = 3.51 \pm 0.01$ with $T_C = 187.67 \pm 0.01$ K for $La_{0.79}Sr_{0.21}CoO_3$, characterizing these second-order phase transitions. For both the crystals, the scaling of the magnetization data above and below T_C obtained using the respective critical exponents and the consistency in the values of the critical exponents determined by different methods confirm that the calculated exponents are unambiguous and intrinsic. The obtained values of exponents suggest that for $La_{0.75}Sr_{0.25}CoO_3$ the transition falls into the three-dimensional Heisenberg universality class of the near-neighbor interaction as proposed for double-exchange systems, whereas in the case of $La_{0.79}Sr_{0.21}CoO_3$ the transition is characterized by mean-field-like values of the critical exponents. We have also estimated the reduced critical amplitudes and observed that for $La_{0.75}Sr_{0.25}CoO_3$ they fall well within the range of the Heisenberg model prediction for spin $S > 1/2$, whereas for $La_{0.79}Sr_{0.21}CoO_3$ they are found to be shifted toward the mean-field values. The deviation of the critical exponents from 3D Heisenberg values toward mean-field ones is attributed to the presence of magnetoelectronic phase inhomogeneity in the $x = 0.21$ single crystal. The detailed analysis of the specific-heat data in the vicinity of T_C for the $x = 0.33$, 0.25, and 0.21 samples also supports the phase separation scenario at around $x = 0.21$.

DOI: 10.1103/PhysRevB.85.214419 PACS number(s): 75.40.Cx, 75.47.Gk, 71.30.+h

I. INTRODUCTION

Although the perovskite cobaltites have relatively less studied as compared to their manganite counterparts, these materials are still an active area of research because of their complex magnetic phase diagram and the presence of an additional degree of freedom, the spin-state transition of the Co ion.[1–15] Among the doped perovskite cobaltites, the prototype large-bandwidth $La_{1-x}Sr_xCoO_3$ (LSCO) system is of particular interest. Besides the spin-glass/cluster-glass behavior, this system exhibits the magnetoelectronic phase separation (MEPS) phenomenon, which refers to the spatial coexistence of multiple electronic and magnetic phases on a nanoscopic length scale even in the absence of chemical segregation.[16–29] The magnetoelectronic phase separation is observed in a large number of doped Mott insulators (e.g., cuprates) and plays a key role in understanding their intriguing physical properties.[30,31] The parent compounds of rare-earth transition metal oxides are magnetoelectronically homogeneous because of the single valence state of the transition-metal ion with antiferromagnetic interaction. When the rare-earth ion is substituted by a group II alkaline-earth ion (e.g., substitution of Sr at the La site in $LaCoO_3$), the system phase-separates into nanoscopic hole-rich metallic clusters in a hole-poor insulating matrix. In $La_{1-x}Sr_xCoO_3$, the MEPS coexists with the spin-state transitions that occur because of the subtle balance between the crystal-field splitting energy and the Hund's coupling energy. The presence of this MEPS in LSCO is well established by different high-resolution experimental techniques.[16–29] Because of the spin-state transitions, in LSCO, the Co^{3+} ion can have a low-spin (t_{2g}^6, $S = 0$), an intermediate-spin ($t_{2g}^5 e_g^1$, $S = 1$), and a high-spin ($t_{2g}^4 e_g^2$, $S = 2$) state and the Co^{4+} ion can have a low-spin (t_{2g}^5, $S = 1/2$), an intermediate-spin ($t_{2g}^4 e_g^1$, $S = 3/2$), and a high-spin ($t_{2g}^3 e_g^2$, $S = 5/2$) state depending on the temperature as well as the value of doping (x).[6–13] The ferromagnetic (FM) double-exchange (DE) interaction Co^{4+}-O-Co^{3+} gives rise to metallic FM clusters and the antiferromagnetic superexchange interaction between the ions of same valence state generates a non-FM semiconducting matrix.[17,32,33] Depending on the value of x, the competing ferromagnetic and antiferromagnetic interactions in coexistence with spin-state transitions make the ground state magnetically inhomogeneous. As the Sr concentration increases, the FM metallic clusters grow in size and number and percolate through the non-FM semiconducting matrix, leading to a crossover from short-range FM to long-range FM metallic state at a percolation threshold $x_p \approx 0.18$.[23,25,34] A detailed study on the size of magnetic cluster and the FM phase fraction in LSCO single crystals reveals that the MEPS is confined to a well-defined doping range, $0.04 < x < 0.22$.[35] Furthermore, in the interval $0.18 < x < 0.22$, the system exhibits a true long-range ferromagnetic ordering but the volume fraction of the FM phase is less than 100%.[35] Samples with $x > 0.22$ exhibit magnetic features similar to that of conventional homogeneous FMs.[35] Thus, in LSCO single crystals, a well-defined doping value $x_c = 0.22$ is set as an upper limit to the region in which this intrinsic

 ©2012 American Physical Society

phase separation exists. Theoretical calculations based on the multiorbital Hubbard model also suggest that the system crosses over from an inhomogeneous phase-separated state to a homogeneous metallic FM state at high doping level.[36] However, in polycrystalline LSCO and related samples, MEPS can occur even up to $x = 0.50$ due to several extrinsic effects.[20–22]

The presence of isolated hole-poor non-FM clusters may introduce compositional disorder in the system. Such disorder has a marked influence on the critical behavior at the FM-paramagnetic (PM) transition as observed in glassy FMs as well as in compositional disordered crystalline FMs.[37,38] Moreover, because of the presence of such non-FM matrix, the percolated FM network has, therefore, a filamentary character which reduces the effective topological dimension of the system. This reduction in the effective dimensionality of the FM network might affect the values of the critical parameters in the asymptotic critical regime (ACR), if the spin-correlation length exceeds the effective dimension of the spin system.[37] This is because the fluctuation effects are important when the physical size of the FM domain is larger than the spin-correlation length in the ACR regime. Even in single crystals with large crystallite size, if the correlation length exceeds the average size of the FM clusters, the fluctuation effect may get suppressed and the true critical behavior is expected to be replaced by the mean-field-like behavior. So, in the FM LSCO single crystal with intrinsic magnetic phase separation, one might expect a different critical behavior from that of a homogeneous FM. This fact led us to investigate the critical behavior of phase-separated as well as homogeneous FM LSCO single crystals.

II. EXPERIMENTAL DETAILS

The polycrystalline powder samples $La_{1-x}Sr_xCoO_3$ ($x = 0.21$ and 0.25) were prepared by standard solid state reaction method using high-purity and preheated La_2O_3, Co_3O_4, and $SrCO_3$ which were mixed in appropriate ratios. The powder materials were repeatedly ground and sintered in air at 1000–1100 °C for a few days. The powder samples were then pressed into cylindrical rods. These rods were finally sintered at 1200 °C for 24 h in a vertical sintering furnace. Single crystals were grown using these rods by the traveling zone method under oxygen atmosphere of 5 bars with a typical growth rate of 4 mm/h. Both the crystals are single phase as checked by powder x-ray diffraction and the Sr contents, determined by energy-dispersive x-ray diffraction, agree within a few percent with the nominal compositions. Single crystallinity was confirmed by the Laue diffraction. The nature of the crystal surface was checked by optical and scanning electron microscopy and no indication of microcracks or segregation was observed. The diffraction pattern of the crystals can be indexed by a rhombohedral unit cell with space group $R\bar{3}c$. The dc magnetization measurements were carried out using a superconducting quantum interference device magnetometer (Quantum Design). All measurements were done with the magnetic field applied parallel to the longest sample dimension to minimize the demagnetization effects. The dc magnetic isotherms in the applied field up to 5 T were measured at an interval of 0.5 K near T_C to locate the critical isotherm and in a 1.0 K interval immediately outside this range. Prior to measurements, the sample was demagnetized by warming to 300 K—well above the ordering temperature—then cooled to the prescribed measuring temperature in the absence of field. The temperature was stabilized for 45 min to allow the sample to reach thermal equilibrium before taking the field-dependent data. The maximum deviation in the temperature was ±5 mK at each measuring temperature. For both the samples, as many as 50 data points were collected for each M-H isotherm using the procedure described above. The demagnetization factor for the sample was determined from the respective low-field linear region of M-H isotherms in the ordered state. All the data used in these analyses were corrected for demagnetization effect. The zero-field specific-heat measurements were done using a standard Quantum Design system (PPMS) via relaxation method.

III. CRITICAL EXPONENTS AND AMPLITUDES

The critical behavior of magnetization and susceptibility near the Curie point of a second-order PM to FM phase transition is characterized by a set of critical exponents (β, γ, and δ) and defined in terms of the dimensionless variable $\varepsilon = (T - T_C)/T_C$ as follows:[39]

$$M_S(0,T) = M_S(0)(-\varepsilon)^{\beta}, \quad \varepsilon < 0, \tag{1}$$

$$\chi_i(0,T) = \chi_0(\varepsilon)^{-\gamma}, \quad \varepsilon > 0, \tag{2}$$

$$M(H,T_C) = A(H)^{1/\delta}, \quad \varepsilon = 0, \tag{3}$$

where $M_S(0,T)$, $\chi_i(0,T)$, and $M(H,T_C)$ are the spontaneous magnetization, initial susceptibility, and magnetization at T_C, respectively, and $M_S(0)$, χ_0, and A are the corresponding critical amplitudes and H is the internal magnetic field. The critical exponents as well as the critical amplitudes exhibit universal behavior near the phase transition point. Based on the dimensionality of the system and the nature of spin-spin interaction, different values for critical exponents are predicted. The critical exponents do not depend on the magnitude of the spin quantum number (S), but the critical amplitudes do so, both on model and spin. In mean-field theory, the reduced amplitudes are given by[39,40]

$$\frac{M_S(0)}{M_0} = \left\{\frac{10(S+1)^2}{3(2S^2+2S+1)}\right\}^{1/2}, \tag{4}$$

$$\frac{\mu_{\text{eff}} H_0}{k_B T_C} = \left\{\frac{30S^2}{(2S^2+2S+1)}\right\}^{1/2}, \tag{5}$$

$$\frac{M_S(0)^{\delta}}{H_0 A^{\delta}} = 1, \tag{6}$$

where M_0 is the zero-temperature saturation magnetization, $H_0 = \chi_0^{-1} M_S(0)$, and $\mu_{\text{eff}} = gS\mu_B$ is the magnetic moment of the fluctuating entity with electronic g factor $g \simeq 2$ and μ_B being the Bohr magneton. Furthermore, according to the scaling hypothesis, the magnetic equation of state for the system is as follows:

$$M(H,\varepsilon) = (\varepsilon)^{\beta} f_{\pm}[H/\varepsilon^{(\gamma+\beta)}], \tag{7}$$

where f_+ for $T > T_C$ and f_- for $T < T_C$ are regular analytical functions.[39] Equation (7) implies that $M|\varepsilon|^{-\beta}$ as a

function of $H|\varepsilon|^{-(\gamma+\beta)}$ produces two universal curves: one for temperatures below T_C and the other for temperatures above T_C with proper choice of β, γ, and δ. This is an important criterion for the accurate and unambiguous values of the critical exponents.

IV. RESULTS AND DISCUSSION

Figure 1(a) shows the temperature dependence of the dc magnetization (M) for the $x = 0.21$ and 0.25 single crystals after cooling at a field of 100 Oe. $M(T)$ shows typical ferromagnetic behavior with T_C's of approximately 188 K and 215 K for $x = 0.21$ and 0.25, respectively, as estimated from the temperature derivatives of $M(T)$ data, which are shown in Fig. 1(b). Both the derivatives exhibit symmetric peaks with respect to their T_C's with full width at half maximum (FWHM) 10.8 K and 4.6 K for $x = 0.21$ and 0.25, respectively. A value of FWHM of ~5 K was observed for the $x = 0.33$ single crystal as shown in our previous report.[41] So, the peak in the dM/dT vs T curve for the $x = 0.21$ sample is two times broader relative to that for the $x = 0.25$ and 0.33 samples. Such a broadening of peak is an indication of magnetoelectronic phase inhomogeneity for the $x = 0.21$ single crystal. The estimated values of the critical temperature for both the samples are in good agreement with that reported in the literature for single-crystalline samples.[34,42] The symmetric nature of the peaks implies good quality and the crystalline nature of the samples.

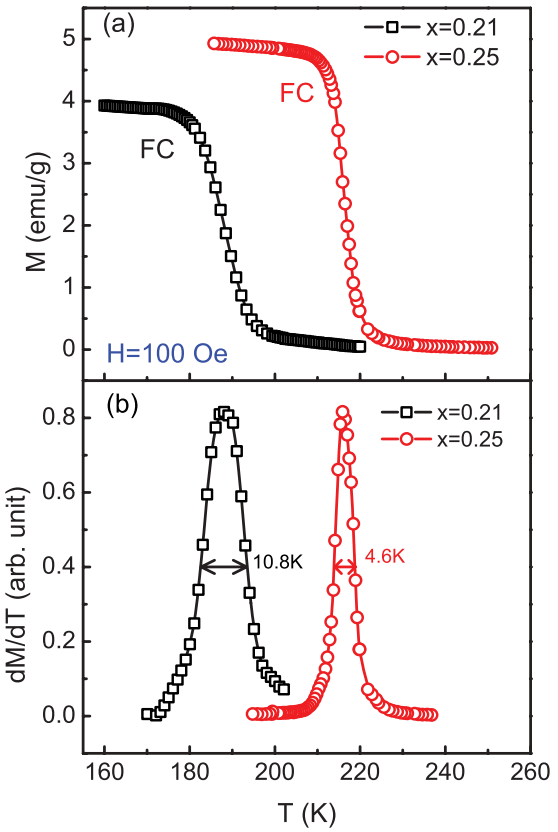

FIG. 1. (Color online) (a) Temperature dependence of field-cooled dc magnetization at 100 Oe of $La_{1-x}Sr_xCoO_3$ single crystals for $x = 0.21$ and 0.25. (b) The temperature dependence of the derivative of dc magnetization data shown in (a) for $x = 0.21$ and 0.25.

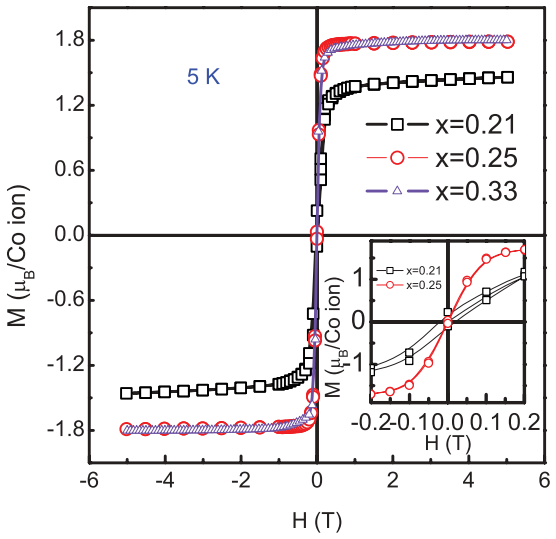

FIG. 2. (Color online) Magnetization hysteresis loops for $x = 0.21$, 0.25, and 0.33 single crystals measured at 5 K. Inset shows the expanded view of the $M(H)$ loops near the low-field region for $x = 0.21$ and 0.25 samples.

Figure 2 shows the magnetization hysteresis loop at 5 K for the $x = 0.21$ and 0.25 single crystals. For comparison, we have also plotted $M(H)$ data for the $x = 0.33$ crystal from our earlier work.[41] For all the samples, magnetization increases sharply with increasing field and essentially saturates in the high-field region with saturated moments of 1.46, 1.76, and 1.8 μ_B/Co ion for $x = 0.21$, 0.25, and 0.33, respectively. The inset of Fig. 2 shows the expanded view of the $M(H)$ loop near the low-field region. It is observed that for $x = 0.25$ the loop is extremely narrow with a coercivity (H_C) approximately 15 Oe, whereas for $x = 0.21$ the hysteresis is relatively larger with H_C approximately 180 Oe but the $M(H)$ loop still has the form of a typical soft ferromagnet. These observations are in good agreement with the earlier reports.[34,42] Also, Fig. 2 shows that the saturation magnetization increases sharply (by 20%) as x increases from 0.21 to 0.25 while it increases marginally (only by 2%) as x increases from 0.25 to 0.33. Thus, it appears that magnetization is sensitive to the hole concentration close to the critical doping level x_c. In the subsequent sections, we will show that such an abrupt decrease in saturation magnetization with the decrease of hole concentration can be explained by taking into account the phase separation scenario for the $x = 0.21$ sample.

Figure 3(a) depicts the temperature dependence of zero-field specific heat (C_p) for $La_{1-x}Sr_xCoO_3$ single crystals with $x = 0.21$, 0.25, and 0.33. For the $x = 0.25$ and 0.33 samples, a clear and large "lambda-like" anomaly is observed at the ordering temperatures, as expected for a second-order FM-PM phase transition. Contrary to this, the $x = 0.21$ sample shows a very weak anomaly at T_C though the ordering is believed to be long-ranged ferromagnetic as it exceeds the percolation threshold x_p. The weakening of this C_p anomaly can be clearly seen from the excess magnetic heat capacity, $C_M(T)$, as shown in the inset of Fig. 3(a). The $C_M(T)$ was

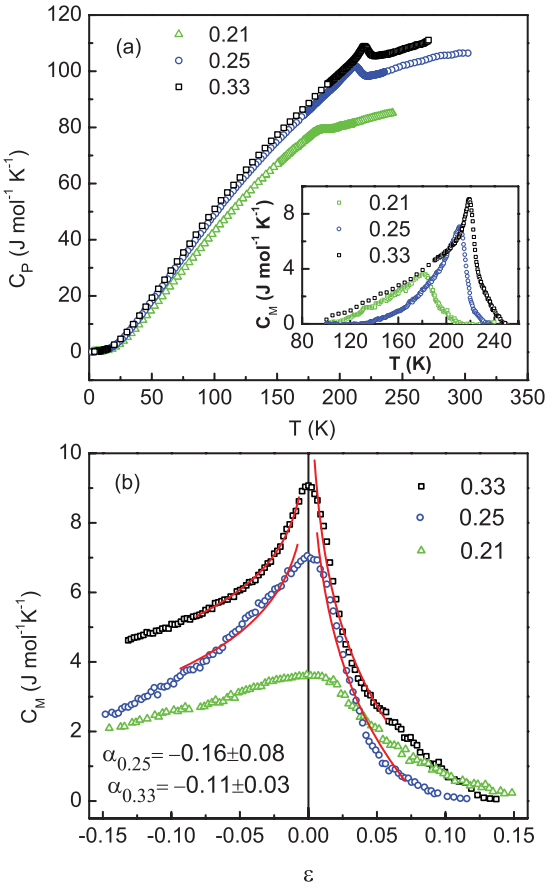

FIG. 3. (Color online) (a) Temperature dependence of the zero-field specific heat for $x = 0.21$, 0.25, and 0.33 single crystals. Inset shows the excess (magnetic) specific heat extracted from the corresponding data by subtracting a smooth background as explained in the text. (b) Magnetic heat capacity in the vicinity of the transition point ($\varepsilon = 0$) for $x = 0.21$, 0.25, and 0.33 single crystals. Solid lines are due to the fit of the functions given by Eqs. (8) and (9) for $x = 0.33$ and 0.25 samples.

calculated by subtracting a smooth background from the measured $C_p(T)$ using a polynomial fit to $C_p(T)$, excluding the region around T_C. Both the height and width of the peak in $C_M(T)$ are very different for the $x = 0.21$ relative to the $x = 0.33$ and 0.25 samples. The peaks are quite sharp for $x = 0.33$ and 0.25, while it is significantly broad and the "lambda-like" feature gets weakened for $x = 0.21$. The anomaly in $C_p(T)$ for the present samples is qualitatively similar to that reported in $La_{1-x}Sr_xCoO_3$ single crystals.[27] For further understanding the nature of the FM-PM transition, we have calculated the magnetic entropy associated with the transition, $S_{\mathrm{Mag}} = \int C_M(T)dT/T$. We observe that S_{Mag} tends to saturate at 2.48, 1.18, and 0.97 J mol^{-1} K^{-1} for $x = 0.33$, 0.25, and 0.21, respectively. These values of S_{Mag} are larger than those reported previously.[27] However, the deduced magnetic entropy is significantly smaller than the expected spin entropy $R\ln(2S+1)$, where S is the spin of the Co ion. The weaker anomaly in $C_p(T)$ and broader peak in the $dM(T)/dT$ curve together with smaller saturation magnetization and larger coercivity are indicative of intrinsic phase inhomogeneity in the $x = 0.21$ single crystal.

The λ-like anomalies (or cusps) in C_M observed at the PM-FM phase transitions occurring near the Curie temperatures for all the samples suggest that the transitions are continuous or second order. For the continuous phase transitions, the specific heat C_P obeys the power law of the reduced temperature, ε, governed by the critical exponents α and α' near $\varepsilon = 0$. In the vicinity of the critical temperature, C_M can be fitted with the following functions:

$$C_M = \frac{A^-}{\alpha'}[(-\varepsilon)^{-\alpha'} - 1] + B^-, \quad \varepsilon < 0, \tag{8}$$

$$C_M = \frac{A^+}{\alpha}[\varepsilon^{-\alpha} - 1] + B^+, \quad \varepsilon > 0, \tag{9}$$

where A^+, A^-, B^+, and B^- are constants and the amplitude ratio A^+/A^- is a universal quantity with large variation between different universality classes.[37,43] Figure 3(b) shows the C_M data close to the transition point ($\varepsilon = 0$). Assuming $\alpha = \alpha'$ as predicted by scaling theory for the continuous phase transition, the least-squares fit of the C_M data to Eqs. (8) and (9) yield a value of critical exponent $\alpha = -0.16 \pm 0.08$ and $A^+/A^- = 2.13 \pm 0.33$ for the $x = 0.25$ single crystal and $\alpha = -0.11 \pm 0.03$ and $A^+/A^- = 2.2 \pm 0.2$ for the $x = 0.33$ single crystal where the uncertainties are the standard errors. The data points very close to the transition point where the transition region is "rounded" have been excluded during the fitting process.[44] The experimental contribution to the rounding of the peak involves the large measuring heat pulses in the relaxation technique[45] and less density of data points close to T_C. The reduced temperature ranges used for the fits are $0.006 \leqslant |\varepsilon| \leqslant 0.08$ for $x = 0.33$ and $0.008 \leqslant |\varepsilon| \leqslant 0.09$ for $x = 0.25$, which lie well inside the $\log|\varepsilon| \leqslant -1.0$ boundary where the observation of true critical behavior is expected.[46] The estimated values of the critical exponent (α) and amplitude ratio (A^+/A^-) for the $x = 0.33$ and 0.25 samples are found to be close to that predicted by the 3D Heisenberg model ($\alpha = -0.115$ and $A^+/A^- = 1.521$).[37] The relatively larger uncertainty in the value of α for $x = 0.25$ than that of $x = 0.33$ is due to the transition region being more rounded in $x = 0.25$ compared to that in $x = 0.33$ as can be seen from Fig. 3(b). The values of the amplitude ratio (A^+/A^-) for the both $x = 0.33$ and 0.25 samples are slightly larger than the 3D Heisenberg value and this may be attributed to the less density of data points close to T_C for $\varepsilon > 0$ and relatively larger ε range used to exclude the "rounded" region. Unlike magnetization, the uncertainty in the estimation of background contribution to the specific heat may be another source of error. Also $\alpha < 0$ implies that C_P exhibits cusplike transition and remains finite at T_C. In contrast, as can be seen from Fig. 3(b), for the $x = 0.21$ sample the rounding of the C_M near and beyond T_C is the most pronounced and shows humplike behavior, which makes meaningful quantitative evaluation of the critical parameters difficult because exclusion of the "rounded" region may involve discarding the data points close to the transition where the critical fluctuation is dominating. The weaker anomaly in C_P and the humplike behavior of C_M near the transition for the $x = 0.21$ single crystal give a clear indication of the presence of intrinsic inhomogeneity in the system.[37,44,47] So the above results indicate that the critical behavior of the pure system is significantly altered in the presence of disorder induced by magnetoelectronic phase

inhomogeneity. In the subsequent sections we have established this from the magnetic measurements as well.

To analyze the critical behavior of the magnetic phase transition, we have used the modified Arrott plot method, based on the Arrott-Noaks equation of state[48]

$$(H/M)^{1/\gamma} = a\left(\frac{T - T_C}{T_C}\right) + bM^{1/\beta}, \qquad (10)$$

where a and b are considered to be constants. The above equation implies that for proper choice of β and γ, the isotherms of the $M^{1/\beta}$ vs $(H/M)^{1/\gamma}$ plot form a set of parallel straight lines and the critical isotherm ($T = T_C$) passes through the origin. The mean-field values of $\beta = 0.5$ and $\gamma = 1$ give the usual Arrott plot (M^2 vs H/M).[49] The deviation from mean-field exponents makes it necessary to use the modified Arrott plot method. An initial choice of β and γ is made from the theoretical models to construct the modified Arrott plot, the isotherms of which may give quasistraight lines. The intercepts of these isotherms on the x and y axes are $1/\chi_i(0,T)^{1/\gamma}$ for $T > T_C$ and $M_S(0,T)^{1/\beta}$ for $T < T_C$, respectively. These $M_S(0,T)$ and $\chi_i(0,T)$ data obtained from the intercepts are tested against the power-law prediction given by Eqs. (1) and (2). With an initial value of T_C obtained from the isotherm that almost passes through the origin of the modified Arrott plot, power laws are fitted following Eqs. (1) and (2) which yield new improved values of T_C, β, and γ. These refined values of β and γ are used to construct a new modified Arrott plot which further gives better values of β, γ, and T_C. This process is repeated until T_C, β, and γ converge to stable values to achieve self-consistency.[37]

Figure 4 shows a series of magnetization isotherms for the $x = 0.21$ sample taken around the Curie temperature. For clarity, we have shown only some selected M versus H plots. These plots show a gradual transition from FM to PM state with increasing temperature. The M^2 versus H/M curves of the Arrott plot (inset of Fig. 4) do not show any negative slope, further confirming that the transition is a continuous

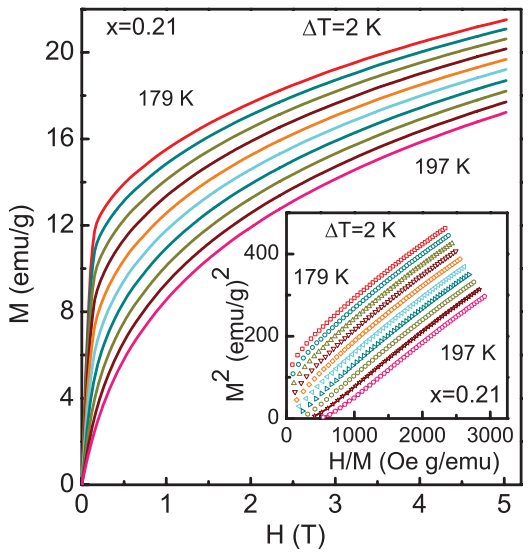

FIG. 4. (Color online) Isothermal magnetization (M vs H) curves at temperatures around T_C of $La_{0.79}Sr_{0.21}CoO_3$. Inset shows the corresponding Arrott plot (isotherms of M^2 vs H/M).

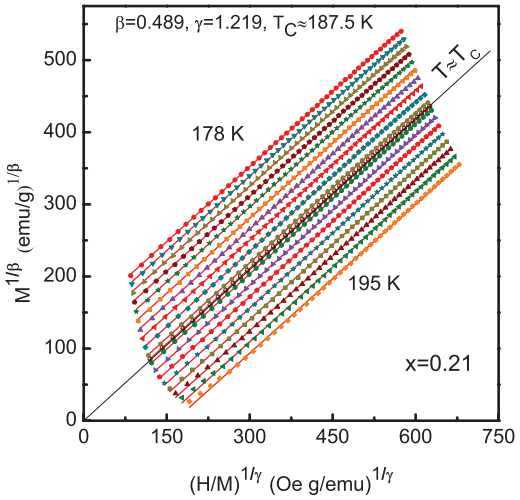

FIG. 5. (Color online) Modified Arrott plot [$M^{1/\beta}$ vs $(H/M)^{1/\gamma}$] isotherms of $La_{0.79}Sr_{0.21}CoO_3$. Solid lines are the high-field linear fit to the isotherms. The isotherm (at $T = 187.5$ K) closest to the Curie temperature ($T_C = 187.67$ K) almost passes through the origin in this plot. All the isotherms measured in the critical region have not been shown for the sake of clarity. Except the critical at $T = 187.5$ K, the temperature interval is 1 K.

or second-order in nature.[50] The isotherms of this Arrott plot are almost parallel straight lines with a weak downward curvature, making it difficult to find the critical isotherm that passes through the origin. So we have constructed the modified Arrott plot as discussed above and the results are shown in Fig. 5. The isotherms in this plot form a set of parallel straight lines for 178 K $\leqslant T \leqslant$ 195 K and 0.1 T $\leqslant H_a \leqslant$ 5 T with the variation in slopes within 1%. During the least-squares fitting to the isotherms, the low-field data below 0.1 T have been excluded because they represent mainly the rearrangement of magnetic domains and also the effect due to the uncertainty in the calculation of demagnetization factor becomes significant in this region. The reduced-temperature range used for these fits is 8×10^{-4} to 3×10^{-2} for $\varepsilon < 0$ and 2×10^{-3} to 4×10^{-2} for $\varepsilon > 0$. The convergence in fitting is achieved for the values of $\beta = 0.489$ and $\gamma = 1.219$. For these values of β and γ, the isotherm for $T = 187.5$ K almost passes through the origin, suggesting $T_C \simeq 187.50$ K which is close to that determined from the dM/dT versus T curve. From the intercepts of the $M^{1/\beta}$ versus $(H/M)^{1/\gamma}$ plots on the x and y axes, we obtain M_S and χ_0^{-1} at different temperatures which are shown in Fig. 6(a). The power-law fit to $M_S(T)$ yields the critical exponent $\beta = 0.485 \pm 0.002$ with $T_C = 187.65 \pm 0.01$ K while to $\chi_0^{-1}(T)$ yields the critical exponent $\gamma = 1.214 \pm 0.004$ with $T_C = 187.67 \pm 0.01$ K where the error bars come from the deviation in the least-squares fit analysis. These values of β, γ, and T_C match very well with that of the modified Arrott plot and, thereby, confirm the self-consistency in the estimates of the exponents and T_C. For further support that the values of the critical exponents and T_C are the correct ones, we have used the Kouvel-Fisher (KF) method,[51]

$$M_S(T)[dM_S(T)/dT]^{-1} = (T_C - T)/\beta, \qquad (11)$$

$$\chi_0^{-1}(T)[d\chi_0^{-1}/dT]^{-1} = (T - T_C)/\gamma. \qquad (12)$$

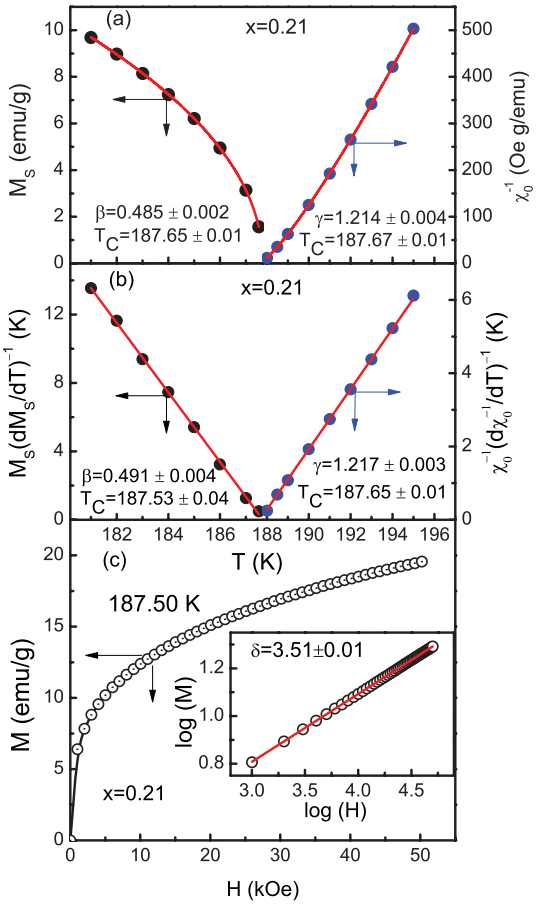

FIG. 6. (Color online) (a) Temperature variation of magnetization $M_S(T)$ and inverse initial susceptibility $\chi_0^{-1}(T)$ along with the fit (solid lines) obtained with the help of power law due to Eqs. (1) and (2) for $x = 0.21$ single crystal. (b) Kouvel-Fisher plot of $M_S(T)$ and $\chi_0^{-1}(T)$. Solid lines are due to the linear fitting of the data. (c) Critical isotherm of M vs H close to the Curie temperature ($T_C = 187.67$ K). Inset shows the same on log-log scale and the straight line is the linear fit following Eq. (3).

According to the above equations, $M_S(T)[dM_S(T)/dT]^{-1}$ and $\chi_0^{-1}(T)[d\chi_0^{-1}/dT]^{-1}$ plotted against temperature yield straight lines with slopes $1/\beta$ and $1/\gamma$, respectively, and they intercept at a point $T = T_C$ on the temperature axis. The linear fit to the plots [Fig. 6(b)] following the KF method gives $\beta = 0.491 \pm 0.004$ with $T_C = 187.53 \pm 0.04$ K and $\gamma = 1.217 \pm 0.003$ with $T_C = 187.65 \pm 0.01$ K. Figure 6(c) shows the critical isotherm for $x = 0.21$, i.e., M versus H plot at temperature 187.5 K, closest to T_C. At $T = T_C$, M and H are related by Eq. (3). The inset of Fig. 6(c) shows the critical isotherm on a log-log plot which should be a straight line with slope $1/\delta$. The linear fit to the plot gives $\delta = 3.51 \pm 0.01$. The three exponents, viz., β, γ, and δ, are related by the Widom scaling relation,[52]

$$\delta = 1 + \frac{\gamma}{\beta}. \tag{13}$$

Using this scaling relation and the estimated values of β and γ from Figs. 6(a) and 6(b), we obtain $\delta = 3.50 \pm 0.01$ and $\delta = 3.48 \pm 0.01$, respectively. These values of δ are very close to the estimated value of δ from the critical isotherm in Fig. 6(c). Thus, the Widom scaling relation is well obeyed by the critical exponents, implying that the values of β and γ are unambiguous and reliable.

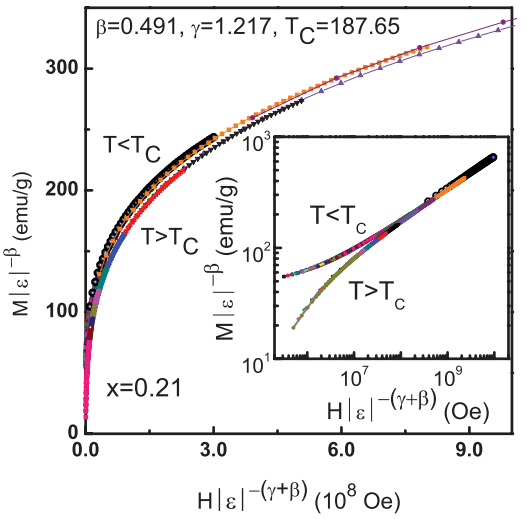

FIG. 7. (Color online) Scaled magnetization of $La_{0.79}Sr_{0.21}CoO_3$ below and above T_C, using β and γ mentioned in the text. The different symbols represent different temperatures. While the linear plot (the main body of this figure) makes evident differences in higher fields, the double-logarithmic plot of the inset reveals differences in the lower fields and also demonstrates the collapse of magnetization isotherms in the critical regime onto the two branches of the scaling function.

The most rigorous method to check the accuracy of the critical exponents and T_C is to compare our data to the prediction of the static-scaling hypothesis following Eq. (7). Using the values of β, γ, and T_C obtained with the KF method, we have plotted $M|\varepsilon|^{-\beta}$ versus $H|\varepsilon|^{-(\gamma+\beta)}$ as shown in Fig. 7. The inset of Fig. 7 shows the same result on a log-log scale. It is clear from the figure that all the isotherms fall onto two different curves, one for $T < T_C$ and the other for $T > T_C$, thus describing the two branches of Eq. (7). The validity of the scaling hypothesis further confirms that the values of the exponents and T_C are unambiguous and self-consistent.

Figure 8 shows the Arrott plot for the $x = 0.25$ sample. As in the case of the $x = 0.21$ sample, the positive slope of the M^2 versus H/M isotherms confirms that the transition is second order. However, the strong downward curvature in the M^2 versus H/M isotherms of the Arrott plot suggests that the critical behavior for this sample is far from mean-field-like. Figure 9 shows the modified Arrott plot, which is constructed with a value of $\beta = 0.365$ and $\gamma = 1.38$ and the isotherm at $T = 214.00$ K almost passes through the origin of this plot, implying $T_C \approx 214.0$ K. The power-law behaviors of the $M_S(T)$ and $\chi_0^{-1}(T)$ data, obtained from the modified Arrott plot, following Eqs. (1) and (2) are shown in Fig. 10(a), which give $\beta = 0.367 \pm 0.002$ with $T_C = 213.94 \pm 0.02$ K and $\gamma = 1.31 \pm 0.01$ with $T_C = 213.97 \pm 0.06$ K. The reduced-temperature range used for these power-law fits is 2×10^{-3} to 4×10^{-2} for $\varepsilon < 0$ and 2×10^{-4} to 3×10^{-2} for $\varepsilon > 0$. The KF plot [Fig. 10(b)] gives $\beta = 0.362 \pm 0.002$ with $T_C = 213.88 \pm 0.06$ K and $\gamma = 1.304 \pm 0.006$ with $T_C = 213.98 \pm 0.02$ K. Figure 10(c) shows the critical isotherm, which gives

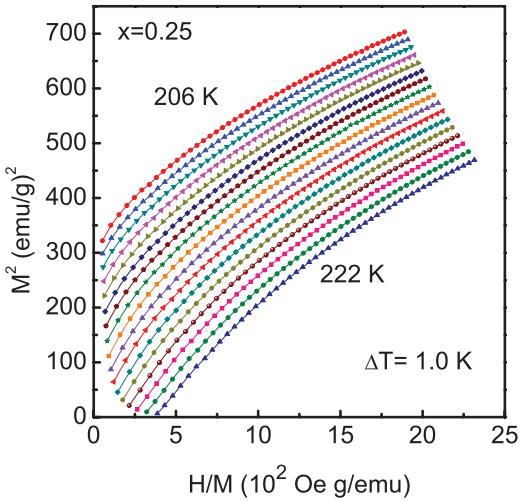

FIG. 8. (Color online) Conventional Arrott plots (M^2 vs H/M) of the magnetization data close to the Curie temperature ($T_C = 214.0$ K) of $x = 0.25$ single crystal.

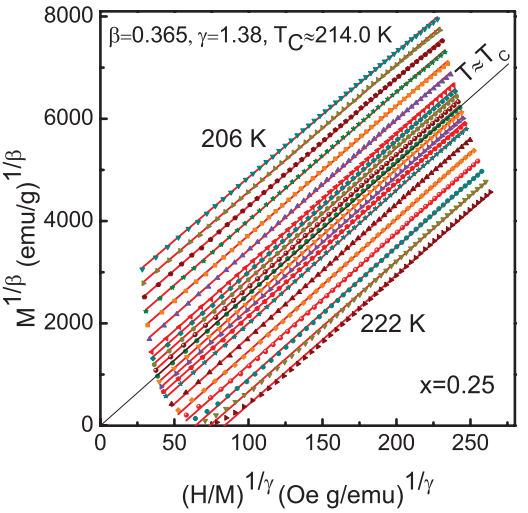

FIG. 9. (Color online) Modified Arrott plot isotherms [$M^{1/\beta}$ vs $(H/M)^{1/\gamma}$] for $x = 0.25$ forming a set of parallel straight lines. The solid lines are the high-field linear fit to the isotherms. The isotherm (at $T = 214.0$ K) nearest to the Curie temperature ($T_C = 213.93$ K) almost passes through the origin in this plot. The temperature interval between 212 K and 216 K is 0.5 K and the rest is in 1 K interval.

the critical exponent $\delta = 4.75 \pm 0.01$ whereas Figs. 10(a) and 10(b) give $\delta = 4.57 \pm 0.01$ and $\delta = 4.60 \pm 0.01$, respectively, following the Widom scaling Eq. (13). Thus the values of δ obtained using different methods are close to each other. This implies that the estimated values of β and γ are reliable and reasonably accurate. Further, the well-obeyed scaling hypothesis (Fig. 11) predicted by Eq. (7) confirms that the values of the exponents as well as T_C are unambiguous and intrinsic to the system. Again, to be sure that the derived exponents for both the samples truly characterize the critical behavior, we have checked whether the above analysis was done within the asymptotic critical regime. To confirm this, we have progressively reduced the temperature range ($|\varepsilon|$) keeping the values of exponents fixed in scaling shown in Figs. 7 and 11 but no visible distortion of the scaling was observed, implying that the fitting processes do not include any point beyond the ACR. The values of the critical exponents for $La_{0.79}Sr_{0.21}CoO_3$, $La_{0.75}Sr_{0.25}CoO_3$, and $La_{0.67}Sr_{0.33}CoO_3$ single crystals, conventional FM (Ni), and the theoretical values based on different models are summarized in Table I for comparison.

Besides estimating the values of the critical exponents to assign a universality class to a system, we have also calculated the reduced critical amplitudes for better understanding the nature of the magnetic properties. Moreover, the analysis of critical amplitudes enables us to determine the effective magnetic moment of the fluctuating entity, which can be compared with experimentally measured parameters of the system such as magnetization. The power-law fit to $M_S(T)$, $\chi_i(T)$, and the critical isotherms following Eqs. (1), (2), and (3), respectively, gives the critical amplitudes $M_S(0)$, χ_0, and A, respectively, which are listed in Table II. The values of the critical amplitudes for $La_{0.79}Sr_{0.21}CoO_3$ are obtained from Figs. 6(a) and 6(c) and those for $La_{0.75}Sr_{0.25}CoO_3$ are obtained from Figs. 10(a) and 10(c). We have also calculated the critical

TABLE I. Comparison of critical parameters of $La_{0.79}Sr_{0.21}CoO_3$ and $La_{0.75}Sr_{0.25}CoO_3$ with earlier reports on cobaltites, conventional ferromagnet Ni, and different theoretical models. Abbreviation: SC, single crystal.

Material	Ref.	Technique	T_C (K)	β	γ	δ
$La_{0.79}Sr_{0.21}CoO_3$ (SC)	This work	Modified Arrott plot	187.6	0.485 ± 0.002	1.214 ± 0.004	3.50 ± 0.01
		Kouvel-Fisher method		0.491 ± 0.004	1.217 ± 0.003	3.48 ± 0.01
		Critical isotherm				3.51 ± 0.01
$La_{0.75}Sr_{0.25}CoO_3$ (SC)	This work	Modified Arrott plot	214.0	0.367 ± 0.002	1.31 ± 0.01	4.57 ± 0.01
		Kouvel-Fisher method		0.362 ± 0.002	1.304 ± 0.006	4.60 ± 0.01
		Critical isotherm				4.75 ± 0.01
$La_{0.67}Sr_{0.33}CoO_3$ (SC)	41	Modified Arrott plot	223.0	0.363 ± 0.002	1.315 ± 0.001	4.62 ± 0.01
		Kouvel-Fisher method		0.361 ± 0.007	1.31 ± 0.001	4.61 ± 0.04
		Critical isotherm				4.64 ± 0.01
Ni	46,54		627.4	0.378 ± 0.004	1.34 ± 0.01	4.58 ± 0.05
3D Heisenberg	37,55–57	Theory		0.365	1.386	4.8
Mean-Field	37,55–57	Theory		0.5	1.0	3.0
3D Ising	37,55–57	Theory		0.325	1.241	4.82

TABLE II. Critical amplitudes of $La_{1-x}Sr_xCoO_3$ single crystals with $x = 0.21$, 0.25, and 0.33 estimated by fitting Eqs. (1)–(3) to the appropriate data. For the $x = 0.33$ sample, we have used our earlier data (Ref. 41). The error bars are due to the best-fit uncertainties.

x	$M_S(0)$ (emu/g)	χ_0 (emu/g Oe)	$A^{-\delta}$ [Oe/(emu/g)$^{\delta}$]
0.21	49.0 ± 0.3	$(4.69 \pm 0.07) \times 10^{-5}$	1.39 ± 0.01
0.25	57.4 ± 0.4	$(2.93 \pm 0.01) \times 10^{-5}$	0.013 ± 0.001
0.33	55.6 ± 0.1	$(2.53 \pm 0.01) \times 10^{-5}$	0.022 ± 0.001

amplitudes for the $La_{0.67}Sr_{0.33}CoO_3$ single crystal from our earlier work and listed them in Table II.[41] M_0 estimated from the low-temperature (5 K) saturation magnetization are 31.1, 42.2, and 43.1 emu g^{-1} for $x = 0.21$, 0.25, and 0.33, respectively. Using these values of M_0, we have calculated the reduced critical amplitudes, which are listed in Table III for comparison with those predicted by different theoretical models.[37,53]

From Table I, one can see that the estimated values of the critical exponents for $La_{0.75}Sr_{0.25}CoO_3$ and $La_{0.67}Sr_{0.33}CoO_3$ single crystals are quite close to those for the 3D Heisenberg model. On the other hand, the exponents for the $La_{0.79}Sr_{0.21}CoO_3$ single crystal are far away from those of the 3D Heisenberg exponents. From Table III, we can also see that the experimentally deduced reduced critical amplitudes $M_S(0)/M_0$ and $A^{-\delta}M_S(0)^{\delta}/H_0$ for the $x = 0.25$ and 0.33 single crystals show satisfactory agreement with the prediction of the Heisenberg model for $S > 1/2$, but clear disagreement with the mean-field theory with both $S = 1/2$ and $S(x)$. However, for the $x = 0.21$ single crystal, $M_S(0)/M_0$ is larger and $A^{-\delta}M_S(0)^{\delta}/H_0$ is smaller than those for the $x = 0.25$ and 0.33 crystals. Table III also shows that these parameters show large deviation from that for Heisenberg model with $S > 1/2$. It is noteworthy that for all three samples the critical amplitude $\mu_{\text{eff}}H_0/k_BT_C$ is smaller than the theoretical prediction and the discrepancy is significant for the $x = 0.21$ sample. We show below that for the $x = 0.21$ crystal a plausible explanation on the basis of the MEPS phenomenon can be given for the mean-field-like high value of β and the strong deviation of the parameter $\mu_{\text{eff}}H_0/k_BT_C$ from the theoretical predicted values.

The estimated values of the reduced critical amplitudes give an important implication regarding the magnetic moment of the fluctuating entity. If H_0 is taken as the effective exchange interaction field and μ_{eff} as the average effective magnetic moment of the fluctuating entity involved in the FM-PM transition, then at $T = T_C$ the effective exchange energy $\mu_{\text{eff}}H_0$ is expected to be equal to the thermal energy k_BT_C. This seems to be the case for the $x = 0.25$ and 0.33 samples when μ_{eff} is identified with $\mu(0)$, the 0 K saturated magnetic moment. From Table III, we see that the estimated values of $\mu_{\text{eff}}H_0/k_BT_C$ are 1.08 and 1.19 for $x = 0.25$ and 0.33, respectively, if we take μ_{eff} as the saturation magnetization at 5 K. However, this is clearly not the case for the $La_{0.79}Sr_{0.21}CoO_3$ single crystal unless μ_{eff} adopts a value much larger than $\mu(0)$. Therefore, in order that $\mu_{\text{eff}}H_0/k_BT_C$ equal the predicated value for any theoretical model, say the Heisenberg model, μ_{eff} needs to be as high as 4.22 μ_B. Several disordered systems exhibit an unusually smaller value of the parameter $\mu_{\text{eff}}H_0/k_BT_C$ as compared to that predicted theoretically.[37,58] According to Kaul[37] and Lago *et al.*,[58] the reason behind this fact is that not all spins but a small fraction of the spins participate in the FM-PM transition. If the concentration of such effective moment is c, then $c = \mu(0)/\mu_{\text{eff}}$ and this fraction of the spins takes part in the transition. A value of $c = 32\%$ has been obtained for the inhomogeneous ferromagnet $SrFe_{0.80}Co_{0.20}O_3$.[58] Because of the existence of non-FM clusters embedded in the percolated ferromagnetic matrix, in the $La_{1-x}Sr_xCoO_3$ system, c is expected to be very sensitive to x close to the percolation threshold and can be significantly smaller than 1. Following the above mentioned prescription, we have estimated c for our samples. The estimated value of c is 35% for the inhomogeneous $La_{0.79}Sr_{0.21}CoO_3$ single crystal. On the other hand, for the ratio $\mu_{\text{eff}}H_0/k_BT_C$ to take the Heisenberg value of 1.58, the values of μ_{eff} become 2.57 μ_B and 2.39 μ_B for $x = 0.25$ and 0.33, respectively. The values of c obtained in this way are 68% and 75% for $x = 0.25$ and 0.33, respectively, which are comparable to the value of $c = 65\%$ for Ni.[37]

The shift in exponents from the 3D Heisenberg (3DH) toward mean field could result from the presence of long-range forces such as isotropic dipolar interactions (IDL). According to RG calculations, a crossover from 3DH to IDL critical behavior occurs at a certain value ε_{co} of reduced temperature

TABLE III. Comparison of reduced critical amplitudes of $La_{1-x}Sr_xCoO_3$ single crystals ($x = 0.21$, 0.25, and 0.33) with those predicted by various theoretical models for a range of spin (S) values. For the $x = 0.33$ sample, we have used our earlier results (Ref. 41). Error bars are due to proportional error and $S(x)$ is the average spin value for the Sr content x deduced from the low-temperature saturation magnetization.

Material	Reduced critical amplitude	Mean field $S = 1/2$, $S = S(x)$	fcc Heisenberg $S = 1/2$, $S = \infty$	fcc Ising $S = 1/2$, $S = \infty$	Expt.
$La_{0.79}Sr_{0.21}CoO_3$	$M_S(0)/M_0$	1.73, 1.68	1.69, 1.22–1.44	1.49, 1.31	1.58 ± 0.02
	$\mu_{\text{eff}}H_0/k_BT_C$	1.73, 2.13	1.58	1.52	0.54 ± 0.03
	$A^{-\delta}M_S(0)^{\delta}/H_0$	1.0	1.55, 1.23–2.07	1.88	1.07 ± 0.04
$La_{0.75}Sr_{0.25}CoO_3$	$M_S(0)/M_0$	1.73, 1.65	1.69, 1.22–1.44	1.49, 1.31	1.36 ± 0.03
	$\mu_{\text{eff}}H_0/k_BT_C$	1.73, 2.32	1.58	1.52	1.08 ± 0.02
	$A^{-\delta}M_S(0)^{\delta}/H_0$	1.0	1.55, 1.23–2.07	1.88	1.52 ± 0.05
$La_{0.67}Sr_{0.33}CoO_3$	$M_S(0)/M_0$	1.73, 1.64	1.69, 1.22–1.44	1.49, 1.31	1.29 ± 0.03
	$\mu_{\text{eff}}H_0/k_BT_C$	1.73, 2.34	1.58	1.52	1.19 ± 0.02
	$A^{-\delta}M_S(0)^{\delta}/H_0$	1.0	1.55, 1.23–2.07	1.88	1.30 ± 0.06

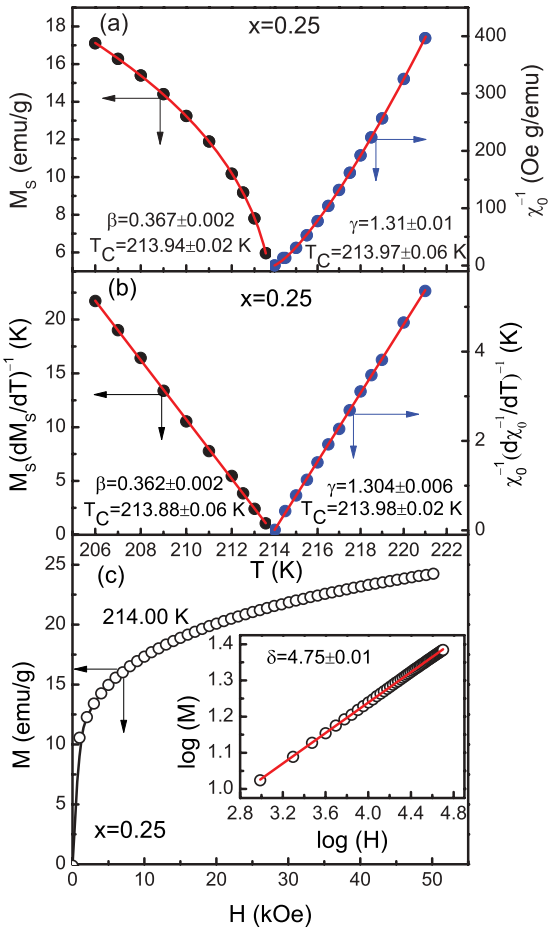

FIG. 10. (Color online) (a) Temperature dependence of spontaneous magnetization $M_S(T)$ and inverse initial susceptibility $\chi_0^{-1}(T)$ along with the fitting curves (solid lines) based on power laws following Eqs. (1) and (2) for $x = 0.25$ single crystal. (b) Kouvel-Fisher plot of $M_S(T)$ and $\chi_0^{-1}(T)$. Solid lines are due to the linear fitting of the data. (c) Critical isotherm of M vs H close to the Curie temperature ($T_C = 213.93$ K). Inset shows the same on log-log scale and the straight line is the linear fit following Eq. (3) giving the value of δ.

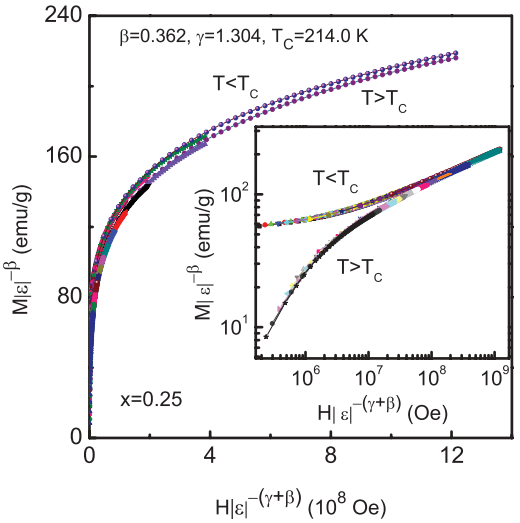

FIG. 11. (Color online) Scaling plot for $La_{0.75}Sr_{0.25}CoO_3$ below and above T_C, using β and γ determined by the KF method. The different symbols represent different temperatures. The inset shows the same on log-log scale exhibiting the collapse of magnetization isotherms in the critical regime onto the two branches of the scaling function. Linear plot emphasizes the difference in high H, whereas log plot emphasizes the difference in low H.

that depends on the strength of the interactions but the values of the exponents characterizing the IDL regime are only marginally different from 3DH values and are shifted toward mean field.[55,59] Such a small shift from 3DH toward mean field has been observed in the inhomogeneous $SrFe_{0.80}Co_{0.20}O_3$ system.[58] But, in the present case, the exponents for the $La_{0.79}Sr_{0.21}CoO_3$ single crystal are very much different from those for 3DH; in fact, they are mean-field-like. Such a deviation from 3DH behavior cannot be explained by IDL perturbations. Furthermore, as nearly the same reduced temperature range (ε) is used in the above analysis for both the samples, the effect of IDL perturbations, if present, should be observed in both the cases. In the $x = 0.25$ sample, no indication of IDL perturbations is observed and the ACR exponents belong to the 3D Heisenberg model. The crossover temperature ε_{co} can be calculated from the relation $\varepsilon_{co} \approx g_d^{1/\phi_d}$,[60] where ϕ_d is the crossover exponent and g_d is the measure of the strength of the dipolar interaction, which can be determined from $g_d \approx \frac{0.87}{T_C}\frac{\theta p^2}{V}$,[59,60] where θ is a correction factor that depends on S, $p = g\sqrt{S(S+1)}$, and V is the unit cell volume in Å^3. We obtain a value of $g_d = 3.3 \times 10^{-4}$ for $x = 0.21$ with $\theta = 0.80$ (following Ref. 60) and $V = 56.3$ Å^3 (Ref. 27 from x-ray diffraction). This gives $\varepsilon_{co} \approx 3.1 \times 10^{-3}$ with $\phi_d \approx \gamma_H = 1.39$.[55,60] Similarly for $x = 0.25$, we deduce $g_d = 3.8 \times 10^{-4}$ and $\varepsilon_{co} \approx 3.5 \times 10^{-3}$. In the present study, as the asymptotic exponents could be determined up to $\varepsilon = 3 \times 10^{-2}$, which is much larger than the ε_{co} for both the samples, the dipolar interactions, if present, have a negligible effect on the critical fluctuations of magnetization.

The deviation of the critical exponents from 3D Heisenberg to mean-field-like values for $x = 0.21$ can be understood from the very nature of the evolution of ferromagnetism in $La_{1-x}Sr_xCoO_3$ single crystals with doping.[35] Neutron diffraction, inelastic neutron spectroscopy, small-angle neutron scattering, magnetization, nuclear magnetic resonance, and heat capacity measurements have established that the LSCO single crystals with $0.04 < x < 0.22$ phase-separate into nanoscopic FM clusters in a non-FM matrix and this MEPS is driven by spatial fluctuations in doping rather than electronically driven.[16–29,35] However, the samples with $x \geqslant 0.22$ exhibit features associated with conventional homogeneous FMs as is observed for the present $x = 0.25$ single crystal. These studies also suggest that the phase-separated samples within the narrow doping zone $0.18 < x < 0.22$ show a true long-range FM ordering with a well-defined T_C but the FM phase fraction is less than one. For the $x = 0.21$ sample, the observed behavior in heat capacity and magnetization are consistent with those reported for samples in the doping range $0.18 < x < 0.22$. Similar to the $x = 0.33$ sample, the estimated values of the critical exponents for the $x = 0.25$ sample are close to that of the 3D Heisenberg model for the isotropic homogeneous FMs with near-neighbor interactions.[41] However, for the $x = 0.21$

single crystal, though the critical exponent β is found to be very close to that for the mean-field model, the value of the critical exponent γ (=1.214) and the temperature dependence of specific heat indicate the presence of severe critical fluctuations for $T \geqslant T_C$. Such a high value of β can be explained within the framework of the Heisenberg model by taking into account the presence of the intrinsic inhomogeneity.[61,62] Using numerical methods, Müller-Krumbhaar[61] investigated the critical behavior of magnetization in a homogeneous Heisenberg spin system with missed spin clusters as the lattice inhomogeneity. They have shown that the local value of β increases close to the missed spin clusters and with the increasing of such missed spin clusters the bulk value of β increases as well. Such an enhancement of β might be related to the weakening of short-range interactions in a lattice randomly diluted with numerous "missing spins." Poon and Durand[62] studied the critical behavior of an amorphous ferromagnet ($Gd_{80}Au_{20}$) and obtained $\beta = 0.44 \pm 0.02$ and $\gamma = 1.29 \pm 0.05$ and explained their results based on this dilution model. So, in our case, for the $x = 0.21$ sample the non-FM clusters or the hole-poor regions might act as missed spin clusters as we have seen earlier that only a small fraction ($c = 32\%$) of the spins take part in the FM-PM transition. The $x = 0.21$ sample may be randomly diluted by such clusters resulting in a weakening of the short-range magnetic interactions leading to a high value of β. The mean-field-like values of the exponents for the $x = 0.21$ sample may also result if the nanoscopic FM clusters embedded in the hole-poor matrix (inhomogeneity) provide an average exchange field in the system which in turn facilitates the FM alignment of bulk magnetic spins in the critical region. The observed critical behaviors for these two samples seem to be consistent with the fact that single-crystalline samples with $x \geqslant 0.22$ behave as conventional homogeneous FMs, whereas samples within the doping range $0.18 < x < 0.22$ contain intrinsic inhomogeneity which has a marked influence in the behavior of the magnetization. Finally, the above analysis further confirms that despite the presence of intrinsic magnetoelectronic phase inhomogeneity, the $La_{0.79}Sr_{0.21}CoO_3$ single crystal exhibits a true long-range ferromagnetism below a well-defined FM-PM phase transition at ~187.6 K.

It is worthy to compare and contrast the evolution of magnetization and the critical behavior of $La_{1-x}Sr_xCoO_3$ with $La_{1-x}Sr_xMnO_3$ (LSMO) close to their percolation thresholds where both the systems turn to FM. The critical observations reveal some important differences in their intrinsic physical properties. Though both the systems behave as DE ferromagnet, unlike $La_{1-x}Sr_xCoO_3$, the ferromagnetic ordering in $La_{1-x}Sr_xMnO_3$ occurs at a much lower Sr doping level ($x \approx 0.10$) than that required for the onset of metallicity ($x \approx 0.17$); i.e., the insulating FM state persists over the range $0.10 \leqslant x \leqslant 0.17$.[10,63] In broadband manganites such as $La_{1-x}Sr_xMnO_3$, $La_{1-x}Ba_xMnO_3$, and $Pr_{1-x}Sr_xMnO_3$, close to their percolation thresholds, the value of saturation magnetization decreases with the increase of x but the FM phase fraction is almost 100%.[10,64,65] Nair *et al.*[66] have studied the critical behavior from bulk magnetization measurements on single-crystalline LSMO with $x = 0.125$ and observed that the values of the exponents match very well with the 3D Heisenberg model. In the FM metallic region, though β for LSMO corresponds to the 3D Heisenberg model, γ is found to lie in between 3D Ising and Heisenberg models.[67] Recent studies on different perovskite manganites show that the critical behavior is consistent with the 3D Heisenberg model.[68–73] Unlike in LSCO, the tendency of intrinsic magnetic phase separation in rare-earth maganites, in general, is much more weaker. Also, there is no consensus on the type and nature of the phase separation and its influence on several electronic and magnetic properties.[30,74] The narrowband manganites that are susceptible to charge-orbital ordering may show nanoscale electronic phase separation. Recently, Asaka *et al.*[75] have used the low-temperature high-resolution transmission electron microscopy involving selected area electron diffraction and Lorentz microscopy in order to obtain crystallographic and magnetic information in both the reciprocal and real spaces of the $La_{0.875}Sr_{0.125}MnO_3$ single crystal. They observed simultaneous evolutions of three charge-modulated phases below 135 K, close to the charge-ordering-transition temperature $T_{CO} = 140$ K. These phases form intricate domain structures within a single ferromagnetic phase; i.e., the system exhibits one and only one magnetic state but multiple charge states. Below 40 K, the three charge-modulated phases behave differently from one another and, as a result, both metallic and insulating electronic phases coexist. This study clearly reveals that the phase separation close to percolation threshold is electronic in nature and the magnetic state remains unaltered. Therefore, $La_{1-x}Sr_xCoO_3$ compounds are the model systems for studying the intrinsic magnetic phase separation which is different from those observed in manganites.

V. CONCLUSION

We have presented a comprehensive study on the critical behavior of magnetic phase transitions in $La_{1-x}Sr_xCoO_3$ single crystals with $x = 0.21$, 0.25, and 0.33 using bulk static magnetization and specific-heat measurements. All the samples undergo a second-order or continuous FM to PM phase transition with a well-defined Curie temperature (T_C). The specific-heat exhibits a sharp and λ-like anomaly at T_C for the $x = 0.25$ and 0.33 single crystals and the estimated values of critical exponent α for these samples are -0.16 ± 0.08 and -0.11 ± 0.03, respectively, which are close to that predicted by the 3D Heisenberg model for isotropic homogeneous FMs. On the contrary, the $x = 0.21$ sample displays a humplike anomaly at T_C, which reflects the inhomogeneous nature of the magnetic ground state. The detailed analysis of magnetization data using different methods such as the modified Arrott plot, KF plot, and critical isotherm suggests that the FM-PM phase transition in the $x = 0.25$ sample is characterized by the 3D Heisenberg critical exponents with near-neighbor interactions, whereas the critical exponents characterizing the phase transition of the $x = 0.21$ single crystal show a large deviation from the 3D Heisenberg values, particularly the critical exponent β, whose value is close to that predicted by the mean-field model. Such a high value of β may result due to the presence of intrinsic inhomogeneity or a hole-poor region which acts as missed spin clusters and weakens the short-range interactions among the spins. Despite the presence of severe critical fluctuations, the behavior of the magnetization deviates from that of a 3D Heisenberg model

due to the observed inhomogeneity in the $x = 0.21$ single crystal. The present study shows that the critical analysis of the phase transition is another sensitive method of probing the magnetoelectronic inhomogeneity in FM $La_{1-x}Sr_xCoO_3$ single crystals. Further studies in this direction with different doping levels and different techniques would be useful to understand the role of intrinsic magnetic inhomogeneity on magnetic phase transition and to reach a consensus on this issue.

ACKNOWLEDGMENTS

The authors would like to thank A. Pal, A. Midya, and D. Bhoi for their help during measurements.

[1]M. A. Señarís-Rodríguez and J. B. Goodenough, J. Solid State Chem. **116**, 224 (1995).
[2]K. Asai, O. Yokokura, N. Nishimori, H. Chou, J. M. Tranquada, G. Shirane, S. Higuchi, Y. Okajima, and K. Kohn, Phys. Rev. B **50**, 3025 (1994).
[3]M. Itoh, I. Natori, S. Kubota, and K. Motoya, J. Magn. Magn. Mater. **140–144**, 1811 (1995).
[4]D. N. H. Nam, K. Jonason, P. Nordblad, N. V. Khiem, and N. X. Phuc, Phys. Rev. B **59**, 4189 (1999); D. N. H. Nam, R. Mathieu, P. Nordblad, N. V. Khiem, and N. X. Phuc, *ibid.* **62**, 8989 (2000).
[5]N. X. Phuc, N. V. Khiem, and D. N. H. Nam, J. Magn. Magn. Mater. **242–245**, 754 (2002).
[6]S. Yamaguchi, Y. Okimoto, and Y. Tokura, Phys. Rev. B **55**, R8666 (1997).
[7]C. Zobel, M. Kriener, D. Bruns, J. Baier, M. Grüninger, T. Lorenz, P. Reutler, and A. Revcolevschi, Phys. Rev. B **66**, 020402 (2002).
[8]K. Asai, P. Gehring, H. Chou, and G. Shirane, Phys. Rev. B **40**, 10982 (1989).
[9]M. A. Korotin, S. Y. Ezhov, I. V. Solovyev, V. I. Anisimov, D. I. Khomskii, and G. A. Sawatzky, Phys. Rev. B **54**, 5309 (1996).
[10]M. Imada, A. Fujimori, and Y. Tokura, Rev. Mod. Phys. **70**, 1039 (1998), and references therein.
[11]M. W. Haverkort, Z. Hu, J. C. Cezar, T. Burnus, H. Hartmann, M. Reuther, C. Zobel, T. Lorenz, A. Tanaka, N. B. Brookes, H. H. Hsieh, H.-J. Lin, C. T. Chen, and L. H. Tjeng, Phys. Rev. Lett. **97**, 176405 (2006).
[12]S. R. English, J. Wu, and C. Leighton, Phys. Rev. B **65**, 220407(R) (2002).
[13]F. Fauth, E. Suard, and V. Caignaert, Phys. Rev. B **65**, 060401 (2001).
[14]K. Mydeen, P. Mandal, D. Prabhakaran, and C. Q. Jin, Phys. Rev. B **80**, 014421 (2009); P. Mandal, P. Choudhury, S. K. Biswas, and B. Ghosh, *ibid.* **70**, 104407 (2004).
[15]I. Fita, R. Szymczak, R. Puzniak, A. Wisniewski, I. O. Troyanchuk, D. V. Karpinsky, V. Markovich, and H. Szymczak, Phys. Rev. B **83**, 064414 (2011); I. Fita, R. Szymczak, R. Puzniak, I. O. Troyanchuk, J. Fink-Finowicki, Ya. M. Mukovskii, V. N. Varyukhin, and H. Szymczak, *ibid.* **71**, 214404 (2005).
[16]P. M. Raccah and J. B. Goodenough, J. Appl. Phys. **39**, 1209 (1968).
[17]M. A. Señarís-Rodríguez and J. B. Goodenough, J. Solid State Chem. **118**, 323 (1995).
[18]R. Caciuffo, J. Mira, J. Rivas, M. A. Señarís-Rodríguez, P. G. Radaelli, F. Carsughi, D. Fiorani, and J. B. Goodenough, Europhys. Lett. **45**, 399 (1999).
[19]R. Caciuffo, D. Rinaldi, G. Barucca, J. Mira, J. Rivas, M. A. Señarís-Rodríguez, P. G. Radaelli, D. Fiorani, and J. B. Goodenough, Phys. Rev. B **59**, 1068 (1999).
[20]P. L. Kuhns, M. J. R. Hoch, W. G. Moulton, A. P. Reyes, J. Wu, and C. Leighton, Phys. Rev. Lett. **91**, 127202 (2003).
[21]M. J. R. Hoch, P. L. Kuhns, W. G. Moulton, A. P. Reyes, J. Wu, and C. Leighton, Phys. Rev. B **69**, 014425 (2004).
[22]M. J. R. Hoch, P. L. Kuhns, W. G. Moulton, A. P. Reyes, J. Lu, J. Wu, and C. Leighton, Phys. Rev. B **70**, 174443 (2004).
[23]J. Wu, J. W. Lynn, C. J. Glinka, J. Burley, H. Zheng, J. F. Mitchell, and C. Leighton, Phys. Rev. Lett. **94**, 037201 (2005).
[24]J. E. Davies, J. Wu, C. Leighton, and K. Liu, Phys. Rev. B **72**, 134419 (2005).
[25]D. Phelan, D. Louca, S. Rosenkranz, S.-H. Lee, Y. Qiu, P. J. Chupas, R. Osborn, H. Zheng, J. F. Mitchell, J. R. D. Copley, J. L. Sarrao, and Y. Moritomo, Phys. Rev. Lett. **96**, 027201 (2006).
[26]V. V. Sikolenko, A. P. Sazonov, I. O. Troyanchuk, D. Többens, U. Zimmermann, E. V. Pomjakushina, and H. Szymczak, J. Phys.: Condens. Matter **16**, 7313 (2004).
[27]C. He, S. Eisenberg, C. Jan, H. Zheng, J. F. Mitchell, and C. Leighton, Phys. Rev. B **80**, 214411 (2009).
[28]D. Louca and J. L. Sarrao, Phys. Rev. Lett. **91**, 155501 (2003).
[29]D. Phelan, D. Louca, K. Kamazawa, S.-H. Lee, S. Rosenkranz, M. F. Hundley, J. F. Mitchell, Y. Motome, S. N. Ancona, and Y. Moritomo, Phys. Rev. Lett. **97**, 235501 (2006).
[30]E. Dagotto, *Nanoscale Phase Separation and Colossal Magnetoresistance* (Springer, New York, 2002).
[31]E. Dagotto, T. Hotta, and A. Moreo, Phys. Rep. **344**, 1 (2001).
[32]V. G. Bhide, D. S. Rajoria, C. N. R. Rao, G. Rama Rao, and V. G. Jadhao, Phys. Rev. B **12**, 2832 (1975).
[33]P. Ganguly and C. N. R. Rao, in *Metallic and Nonmetallic States of Matter*, edited by P. P. Edwards and C. N. R. Rao (Taylor & Francis, London, 1985).
[34]H. M. Aarbogh, J. Wu, L. Wang, H. Zheng, J. F. Mitchell, and C. Leighton, Phys. Rev. B **74**, 134408 (2006).
[35]C. He, S. El-Khatib, J. Wu, J. W. Lynn, H. Zheng, J. F. Mitchell, and C. Leighton, Europhys. Lett. **87**, 27006 (2009).
[36]R. Suzuki, T. Watanabe, and S. Ishihara, Phys. Rev. B **80**, 054410 (2009).
[37]S. N. Kaul, J. Magn. Magn. Mater. **53**, 5 (1985).
[38]H. Maletta, G. Aeppli, and S. M. Shapiro, J. Magn. Magn. Mater. **31–34**, 1367 (1983).
[39]H. Eugene Stanley, *Introduction to Phase Transitions and Critical Phenomena* (Oxford University Press, New York, 1971).
[40]W. Li, H. P. Kunkel, X. Z. Zhou, G. Williams, Y. Mukovskii, and D. Shulyatev, Phys. Rev. B **70**, 214413 (2004).
[41]N. Khan, A. Midya, K. Mydeen, P. Mandal, A. Loidl, and D. Prabhakaran, Phys. Rev. B **82**, 064422 (2010).
[42]M. Kriener, C. Zobel, A. Reichl, J. Baier, M. Cwik, K. Berggold, H. Kierspel, O. Zabara, A. Freimuth, and T. Lorenz, Phys. Rev. B **69**, 094417 (2004).

[43]F. L. Lederman, M. B. Salamon, and L. W. Shacklette, Phys. Rev. B **9**, 2981 (1974).
[44]A. Kornblit and G. Ahlers, Phys. Rev. B **11**, 2678 (1975).
[45]J. C. Lashley, M. F. Hundley, A. Migliori, J. L. Sarrao, P. G. Pagliuso, T. W. Darling, M. Jaime, J. C. Cooley, W. L. Hults, L. Morales, D. J. Thoma, J. L. Smith, J. Boerio-Goates, B. F. Woodfield, G. R. Stewart, R. A. Fisher, and N. E. Phillips, Cryogenics **43**, 369 (2003).
[46]L. P. Kadanoff, W. Götze, D. Hamblen, R. Hecht, E. A. Lewis, V. V. Palciauskas, M. Rayl, J. Swift, D. Aspnes, and J. Kane, Rev. Mod. Phys. **39**, 395 (1967).
[47]J. A. Souza, J. J. Neumeier, B. D. White, and Yi-Kou Yu, Phys. Rev. B **81**, 172410 (2010).
[48]A. Arrott and J. E. Noakes, Phys. Rev. Lett. **19**, 786 (1967).
[49]A. Arrott, Phys. Rev. **108**, 1394 (1957).
[50]B. K. Banerjee, Phys. Lett. **12**, 16 (1964).
[51]J. S. Kouvel and M. E. Fisher, Phys. Rev. **136**, A1626 (1964).
[52]B. Widom, J. Chem. Phys. **43**, 3898 (1965); **41**, 1633 (1964).
[53]S. Milosevíc and H. E. Stanley, Phys. Rev. B **6**, 986 (1972); **6**, 1002 (1972); R. Krasnow and H. E. Stanley, *ibid*. **8**, 332 (1973); C. Domb and M. S. Green, *Phase Transitions and Critical Phenomena* (Academic, New York, 1974).
[54]J. S. Kouvel and D. S. Rodbell, Phys. Rev. Lett. **18**, 215 (1967).
[55]M. Seeger, S. N. Kaul, H. Kronmüller, and R. Reisser, Phys. Rev. B **51**, 12585 (1995).
[56]C. Bagnuls and C. Bervillier, Phys. Rev. B **32**, 7209 (1985).
[57]V. Privman, P. C. Hohenberg, and A. Aharony, in *Phase Transitions and Critical Phenomena*, edited by C. Domb and J. L. Lebowitz (Academic, New York, 1991), p. 1.
[58]J. Lago, M. J. Rosseinsky, S. J. Blundell, P. D. Battle, M. Diaz, I. Uriarte, and T. Rojo, Phys. Rev. B **83**, 104404 (2011).
[59]A. Aharony and M. E. Fisher, Phys. Rev. B **8**, 3323 (1973); M. E. Fisher and A. Aharony, Phys. Rev. Lett. **30**, 559 (1973).
[60]K. Ried, D. Köhler, and H. Kronmüller, J. Magn. Magn. Mater. **116**, 259 (1992).
[61]H. Müller-Krumbhaar, J. Phys. C **9**, 345 (1976).
[62]S. J. Poon and J. Durand, Phys. Rev. B **16**, 316 (1977).
[63]J. Wu and C. Leighton, Phys. Rev. B **67**, 174408 (2003).
[64]P. Mandal and B. Ghosh, Phys. Rev. B **68**, 014422 (2003).
[65]C. Martin, A. Maignan, M. Hervieu, and B. Raveau, Phys. Rev. B **60**, 12191 (1999).
[66]S. Nair, A. Banerjee, A. V. Narlikar, D. Prabhakaran, and A. T. Boothroyd, Phys. Rev. B **68**, 132404 (2003).
[67]K. Ghosh, C. J. Lobb, R. L. Greene, S. G. Karabashev, D. A. Shulyatev, A. A. Arsenov, and Y. Mukovskii, Phys. Rev. Lett. **81**, 4740 (1998).
[68]J. Fan, L. Ling, B. Hong, L. Zhang, L. Pi, and Y. Zhang, Phys. Rev. B **81**, 144426 (2010), and references therein.
[69]B. Padmanabhan, H. L. Bhat, S. Elizabeth, S. Rößler, U. K. Rößler, K. Dörr, and K. H. Müller, Phys. Rev. B **75**, 024419 (2007).
[70]J. Yang, Y. P. Lee, and Y. Li, Phys. Rev. B **76**, 054442 (2007), and references therein.
[71]W. Jiang, X. Z. Zhou, G. Williams, Y. Mukovskii, and K. Glazyrin, Phys. Rev. B **77**, 064424 (2008).
[72]P. Sarkar, S. Arumugam, P. Mandal, A. Murugeswari, R. Thiyagarajan, S. Esaki Muthu, D. Mohan Radheep, C. Ganguli, K. Matsubayshi, and Y. Uwatoko, Phys. Rev. Lett. **103**, 057205 (2009).
[73]S. Rößler, Harikrishnan S. Nair, U. K. Rößler, C. M. N. Kumar, S. Elizabeth, and S. Wirth, Phys. Rev. B **84**, 184422 (2011).
[74]M. Uehara, S. Mori, C. H. Chen, and S.-W. Cheong, Nature (London) **399**, 560 (1999).
[75]T. Asaka, S. Mori, Y. Horibe, K. Takenaka, X. Z. Yu, T. Nagai, K. Kimoto, T. Hirayama, and Y. Matsui, Phys. Rev. B **83**, 174401 (2011).